

Surface charging of a crater near lunar terminator

A K Anuar

Department of Communication Engineering, Faculty of Electrical and Electronic Engineering,
Universiti Tun Hussein Onn Malaysia, 86400 Parit Raja, Johor, MALAYSIA

E-mail: abul@uthm.edu.my

Abstract. Past lunar missions have shown the presence of dust particles in the lunar exosphere. These particles originate from lunar surface and are due to the charging of lunar surface by the solar wind and solar UV flux. Near the lunar terminator region, the low conductivity of the surface and small scale variations in surface topology could cause the surface to charge to different surface potentials. This paper simulates the variation of surface potential for a crater located in the lunar terminator regions using Spacecraft Plasma Interaction Software (SPIS). SPIS employs particle in cell method to simulate the motion of solar wind particles and photoelectrons. Lunar crater has been found to create mini-wake which affects both electron and ion density and causes small scale potential differences. Simulation results show potential difference of 300 V between sunlit area and shadowed area which creates suitable condition for dust levitation to occur.

1. Introduction

The transport of dust particles over the lunar atmosphere has been observed by astronauts during the Apollo missions and is believed to be the cause of *horizon glow* [1]. The first evidence of dust transport across the lunar surface was gathered by the Apollo 17's Lunar Ejecta and Meteorite (LEAM) experiment suggesting both vertical and horizontal dust transport particularly around the terminator region [2]. These lifted dust particles can be a major environmental hazard to any space activities on lunar surface. Major effects include reduced equipment lifetime due to adhesion and abrasion, reduction in optical visibility due to dust levitation, astronaut's health hazards and contamination of solar panels [3].

The transport of dust particle is believed to be due to the charging of the lunar surface by the ambient solar wind plasma and other charging process such as photoemission which create repelling electrostatic force between the dust particle and the surface [4]. It is therefore important to understand the charging process of the surface, in particular near the area where increase dust particle flux has been observed. Recently, a new particle in cell code has been developed with the capability of simulating surface charging and dusty plasma in the lunar environment [5, 6]. This paper presents simulation of the lunar surface charging over the lunar terminator region using the code.

2. Lunar surface charging

Surface interactions with solar wind plasma and UV radiation causes the lunar surface to become electrically charged with the process has been investigated since the early years of Apollo missions. In general, the charging of the lunar surface begins with the collection of incident solar wind particles



and emission of secondary electrons and photoelectrons which will charge the surface to a floating potential. The current balance equation for the charging process is given by

$$I_e = I_i + I_{se} + I_{ph} \quad (1)$$

where I_e , I_i , I_{se} , I_{ph} are electron, ion, secondary electron and photoemission current respectively [4].

The resulting potential depends on which of these 4 main sources is dominant and is not consistent over the whole lunar surface because of the low surface conductivity with small scale variations have been observed and reported in many previous works (see for example [7]). On a large spatial scale, the sunlit side is charged to positive potential due to photoelectrons while the night side charges to negative potential as ions and solar UV flux are being screened by the lunar body.

In the presence of solar UV flux, incidence photons excite electrons on the surface, emitting them as low energy ($E_{ph} \sim 2 \text{ eV}$) photoelectrons. This process is highly dominant on the dayside of the lunar surface with the photocurrent exceeds the ambient electron current, thus charging the surface to positive potential. On the night side however, the absence of solar UV photons and the screening of solar wind protons mean the main charging current is the high energy electrons which are the first to enter the cavity due to their higher thermal speed. These high energy electrons charge the surface to high negative potential in order to attract more solar wind ions into the cavity, as well as preventing more electrons from reaching the surface. Figure 1 shows current collection and surface potential of a flat surface in the lunar terminator region. The absence of photoemission due to solar UV flux charges the surface to negative potential, as opposed to positive potential often observed in daylight region.

2.1. Lunar terminator region

Halfway between the sunlit and the night side region is the terminator region, where lunar surface is exposed to near parallel solar wind flow with very little or no solar UV flux. At this region, the main charging current comes from the ambient solar wind plasma but local surface topology such as crater and boulder could create localized regions of positive and negatively charged surfaces [7]. These localized regions are more prevalent in the terminator region because the almost parallel approach of solar wind and solar UV flux means a simple structure such as a boulder or a crater would have had a significantly shadowed region.

A crater at this region for example will have one side of the crater's rim obscured from both solar wind and solar UV flux, with the opposite with are accessible to both, creating a shadowed region. The shadowed region can be described as *mini wake* because it acts in a similar way as the lunar wake, i.e. it has depleted ion density and no photoemission [7]. As the lunar surface is full of craters and boulders, it is possible to have potential variations around these structures which would complicate the effort to understand the lunar exosphere. On a large scale however, lunar surface in the terminator region is charged to $\sim -70 \text{ eV}$ with the transition from positively charge dayside surface to negatively charge nightside surface happen inside the dayside region due to reduced solar wind and solar UV induced currents (ion and photoemission current) [7].

The potential developed on the lunar surface due to the charging processes creates a non-neutral layer of plasma sheath which screens either electrons or ions, creating a density gradient which in turn leads to electric field on the surface. On the night side, the electric field is directed towards the surface which accelerates ions onto the surface. The opposite happens on the dayside, where the field is directed outward and accelerates electrons towards the surface. The plasma sheath layer, assuming a Maxwellian velocity distribution for electrons can be described by

$$\Phi(z) = -\Phi_0 \exp\left(\frac{z}{\lambda_D}\right) \quad (2)$$

where Φ_0 is the potential bias of the surface, λ_D is the plasma Debye length ($\lambda_D = \sqrt{\frac{\epsilon_0 k_B T}{n_0 e^2}}$) and z is the distance normal from the surface.

3. Simulation parameters

Spacecraft Plasma Interaction Software (SPIS) which employs particle-in-cell (PIC) method [9] has been upgraded to allow lunar surface charging to be investigated [5]. In addition to simulating the motion of solar wind particle, the code also allows simulation of photoemission originating of the surface which has been found to be one major charging current especially in the dayside region. Photoemission and photoelectrons are modelled using a similar model to the one proposed by [10]. The 3-dimensional and unstructured mesh employed by SPIS allows close representation of the lunar surface topology which is suited to this study.

SPIS is employed to model the lunar charging process using plasma parameters given by [8], where $n_e \sim n_i = 10^7 \text{ m}^{-3}$ and $T_e \sim T_i = 10 \text{ eV}$ with Maxwellian velocity distribution and ion drift velocity of $v_{sw} \sim 400 \text{ km} \cdot \text{s}^{-1}$. Simulation is first performed for a flat lunar surface over an area $6\lambda_D \times 6\lambda_D$ where $\lambda_D = 7.5 \text{ m}$ is the solar wind plasma Debye length. At terminator, it has been assumed that there is no photoemission from the surface due to very low exposure to solar UV. Figure 1 shows the current collection for ions and electrons and the resulting surface potential. Surface is found to have charged to around $\sim -60 \text{ V}$ after approximately 2 ms.

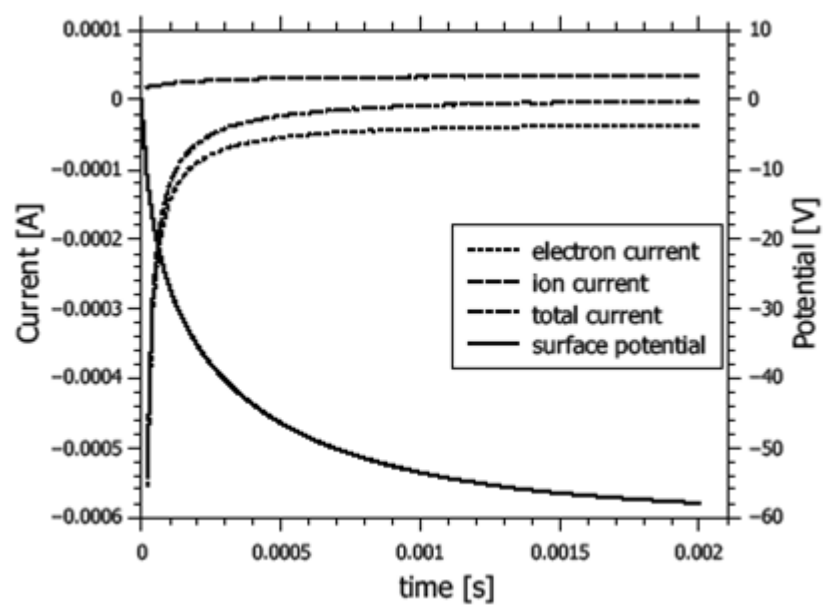


Figure 1. Current collection and surface potential for a surface near the terminator region. No photoemission in this region charges the surface to negative potential.

4. Surface charging near lunar terminator

Surface topography plays an important role in charging process and could produce localized potential difference [7]. Structures such as crater and boulder could disturb the natural solar wind flow and solar UV flux creating shadowed region. This shadowed region is charged to different potential than the

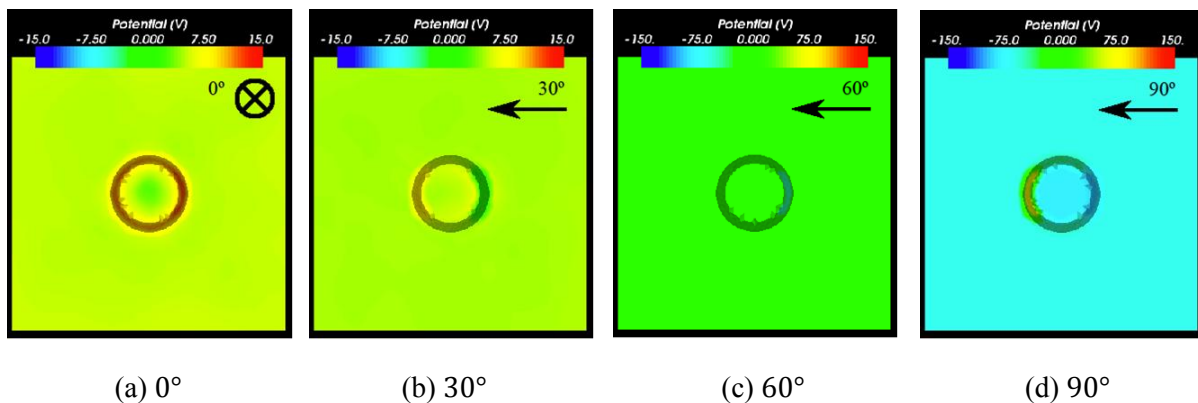


Figure 2. Surface potential around a 1-m depth, 5-m diameter crater for (a) 0° , (b) 30° , (c) 60° and (d) 90° solar wind incidence angle.

illuminated region where the effects is more prevalent near the terminator region due to the low sun angle. In the simulation, charging process are observed for 4 solar wind and solar UV illumination angles which are 0° , 30° , 60° and 90° .

Figure 2 shows the potential of a 1-m deep, 5 meter in diameter crater for the 4 sun incidence angles. In Figure 2(a), the whole surface of the crater is exposed to the solar wind and solar flux. Potential difference is observed between the crater rim and the rest of the surface. In Figure 2 (b), opposite edges of the crater are charged to opposite polarity. The edge in blue is the ones in shadow which is charged to negative potential because solar wind photons are being obstructed by the crater's rim. The side facing the solar wind is charged to $\sim 9\text{ V}$ while the one in shadowed is charged to -3 V . In Figure 2(c), the low solar angle has reduces the flux to the shadowed side even further with the surface is charged to $\sim -70\text{ V}$. In Figure 2(d), surface facing the solar wind is charged to positive potential while the one in shadow is charged to negative potential. A potential close to $\sim -100\text{ V}$ can be seen on the shadowed side.

4.1 Electron and ion densities

Figure 3 shows the densities and potential across a crater located at 90° from the sub solar point. In Figure 3(a), the electron density near the crater is reduced to almost 3 order of magnitude smaller due to the strong electric field created by the negatively charged surface. Further electron depletion can be observed at the shadowed region inside the crater where density dropped to 10^2 m^{-3} which is due to the strong potential barrier. In comparison, ion density in the area outside the crater is almost constant over the surface with its density approximately the same as its ambient density ($n_i \sim 10^7\text{ m}^{-3}$), as shown in Figure 3(b). However, near the shadowed region inside the crater, the density is reduced to almost zero as most of the subsonic ions are completely obscured from the region. This causes the surface to charge to high negative potential as there is no ions to help lowering the magnitude of the surface potential. On the other hand, surface facing the shadowed region is charged to positive potential as ions are being collected by the surface. The surface and plasma potential are shown in Figure 3(c).

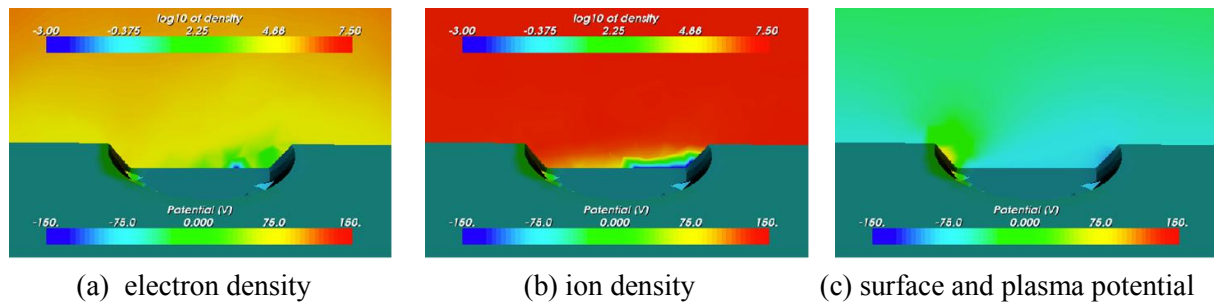


Figure 3. Plasma density and potential near crater at 90° .

4.2 Energetic solar wind plasma

Solar wind density and temperature are two parameters that could result in different potential level than the one observed in the preceding simulations. These two parameters vary over time and are highly dependent on solar activities. A simulation is performed for the case of crater near terminator ($\theta = 90^\circ$) in a more energetic solar wind plasma. The average temperature of the solar wind is doubled from 10 eV to 20 eV and the remaining parameters of the simulation are retained.

Figure 4(a) and (b) show the surface and plasma potential for the crater after approximately 50 ms of simulation time. In Figure 4(a), the area outside the crater is charged to ~ -90 V while the base of the crater is charged to ~ -100 V. Having more energetic populations results in higher negative surface potential and is largely due to the increase in electron thermal energy. As for ions, since their motion are largely dominated by the subsonic flow, they would contribute approximately the same charging current to the surface under these conditions.

In Figure 4(a), the area outside the crater reaches its equilibrium potential after approximately 10 ms of simulation time whilst the one in shadow has yet to reach its equilibrium potential after 50 ms. The slow charging process of the shadowed surface is due to the lack of thermal ions reaching the surface. It is predicted that the surface will continue to charge to higher negative potential in order to attract more ion particles to the surface. It is also believed that an increase in solar wind speed would only result in a more negative patch since ions will have larger horizontal velocity component, and thus are more likely to be shielded by the crater's edge.

In addition to the high negative potential found on the shadowed crater's rim, a small patch of highly negative surface can be seen appearing near the top of the positively charged crater's rim. The formation of this patch is believed to be the result of screening of ions by the positively charged sun-facing crater's rim. The positive barrier shown in Figure 4(b) causes incoming ions to be deflected over the area which is indicated by the slightly high ion density near the patch (see Figure 4(c)). This patch also repels incoming electrons creating small region of reduced electron density as illustrated in Figure 4(d).

4.3 Bi-Maxwellian solar wind

The solar wind near lunar surface is more likely to contain both the fast and slow solar wind components. A simulation is performed for the case of crater for this type of plasma condition where the slow solar wind component is made of plasma with $n_s = 10^6 \text{ m}^{-3}$ and $T_s = 10$ eV whilst the fast solar wind is set to $n_f = 5 \times 10^6 \text{ m}^{-3}$ and $T_f = 20$ eV. The streaming speed for both slow and fast solar wind are set to $400 \text{ km} \cdot \text{s}^{-1}$ and $700 \text{ km} \cdot \text{s}^{-1}$ respectively. Figure 5 shows the surface potential obtained from the simulation. From the figure, it is obvious that a similar pattern of surface potential can be observed near the lunar crater where the side in shadow is charged to negative potential whilst the one facing the solar wind is charged to positive potential. The simulation indicates an increase in the magnitude of the surface potential on both sides of the crater (shadowed and sunlit) but within the range anticipated by [8]. The simulation shows that there is around 200 V difference between the side in shadow and the one facing the solar wind which could create strong electric field. The changes in

surface potential also confirm the time varying nature of lunar surface potential with regards to the change in solar wind plasma properties.

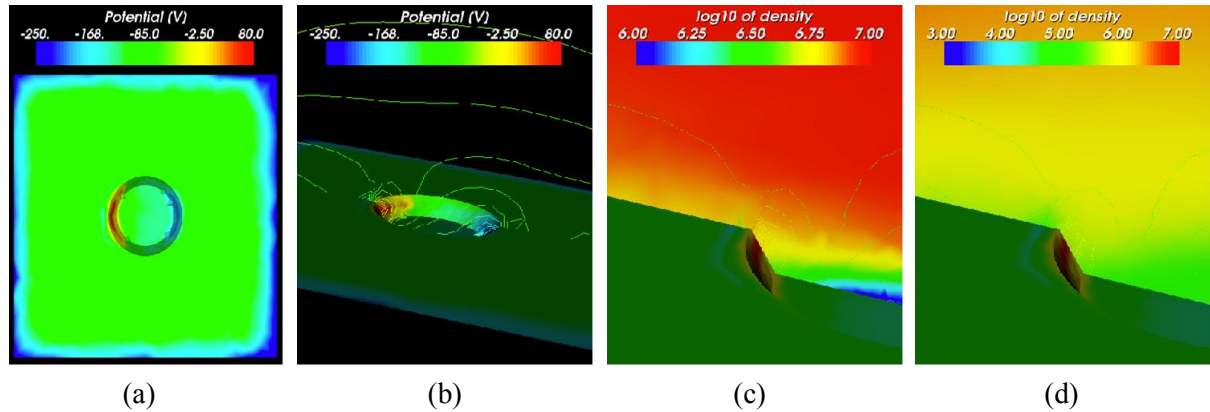


Figure 4. Potential and species densities of a crater for $TeV = 20$ eV for (a) surface potential, (b) plasma potential, (c) ion density and (d) electron density.

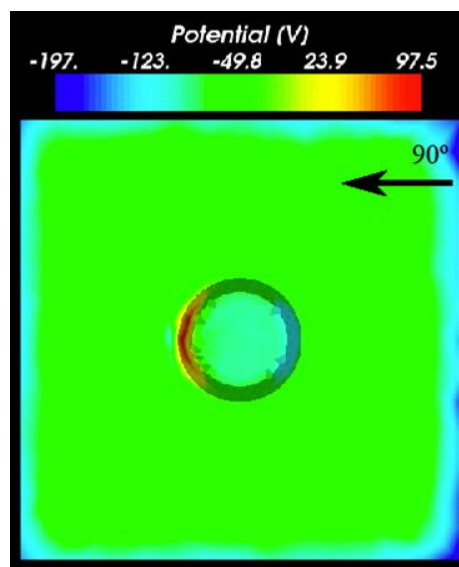


Figure 5. Surface potential near a crater for Bi-Maxwellian solar wind distribution.

5. Conclusion

Results obtained show the capability of SPIS in simulating the lunar surface charging process. Near the lunar terminator, the parallel approach of the solar wind and solar UV causes the surface to be negatively charged due to lack of photoemission current. Surface topology such as crater could charge the surface to different charging potentials with the solar wind facing surface is charged to positive potential while the shadowed surface is charged to negative potential. Potential difference of about 200 V can be observed and could increase in the presence of more energetic and bi Maxwellian solar wind plasma. This high negative potential has been shown to be able to levitate dust particles which could create a dusty lunar exosphere.

References

- [1] Criswell D R 1972 Horizon-glow and motion of lunar dust *Abstracts of the Lunar and Planetary Science Conference* **3163**
- [2] Berg O, Wolf H and Rhee 1976 j Lunar soil movement registered by the Apollo 17 cosmic dust experiment. *Interplanetary dust and zodiacal light* 233
- [3] Christofoersen R, Lindsay J F, Noble S K *et al.* 2009 Dust Effects on Spacesuit Systems: Insight from Apollo Spacesuits, NASA/TP-2009-214786, Johnson Space Center, Houston, Texas
- [4] Manka R H 1973 Plasma and Potential at the Lunar Surface. In R. J. L. Garard, editor, Photon and Particle Interactions with Surfaces in Space *Astrophysics and Space Science Library* **37** 347
- [5] Anuar A K 2013 Honary F, Hapgood M and Roussel J -F 2013 Three dimensional simulation of dust charging and dusty plasma using SPIS *J. Geophys. Res.: Space Phys.* **118**(10) 6723
- [6] Hess S L G and Sarrailh P, Mat_eo-V_elez J -C *et al.* 2015 New SPIS capabilities to simulate dust electrostatic charging, transport, and contamination of lunar probe *IEEE Trans. Plasma Sci.* **43**(9) 2799
- [7] Farrell W M, Stubbs T J, Halekas J S *et al.* 2008 Loss of solar wind plasma neutrality and affect on surface potentials near the lunar terminator and shadowed polar regions *Geophys. Res. Lett.* **35**(5) L05105
- [8] Colwell J E, Batiste S, Horanyi M, Robertson S and Sture s 2007 Lunar surface: Dust dynamics and regolith mechanics *Rev. Geophys.* **45**(2) RG2006
- [9] Roussel J -F, Rogier F, Dufour G *et al* 2008 SPIS open-source code: Methods, capabilities, achievements, and prospects. *IEEE Trans. Plasma Sci.* **36**(5) 2360
- [10] Poppe A and Horanyi M 2010 Simulations of the photoelectron sheath and dust levitation on the lunar surface *J. Geophys. Res.* **115** A08106